The effects of confinement and wettability on the phase behavior of pure and multicomponent fluids in nanoporous media

An T. T. Nguyen and Mohammad Piri*

Center of Innovation for Flow through Porous Media, Department of Energy and Petroleum Engineering, University of Wyoming, Laramie, WY 82071, USA

Abstract. The phase behavior of fluids stored in nanopores deviates significantly from bulk behavior due to intense molecular interactions in confined spaces. Understanding these confinement-induced effects is essential for applications such as carbon capture using nanoporous materials, gas storage, and enhanced hydrocarbon recovery in unconventional reservoirs. While most geological formations contain multicomponent fluid systems, existing studies typically focus on the phase behavior of single-component fluids. As a result, the phase behavior of mixtures under confinement remains poorly understood. This knowledge gap limits the evaluation of fluid storage in nanoporous media, particularly storing fluid mixtures in materials with varying wettability. In such systems, fluid-solid interactions can lead to distinct phase behavior in mixtures compared to pure fluids. The present study addresses this gap by investigating the thermodynamic behavior of pure carbon dioxide at 10 °C and an n-butane/n-hexane binary mixture (90 mol% n-butane) at 10, 20, and 30 °C in Mobil Composition of Matter No. 41 (MCM-41) nanoporous materials. Adsorption and desorption isotherms were measured in hydrophilic and hydrophobic MCM-41 samples with a pore size of 8 nm using a patented nano-condensation apparatus. The results show that the adsorption behavior of the fluid mixture closely resembles that of pure carbon dioxide, with higher storage capacities in hydrophilic samples. However, desorption behavior, critical for hydrocarbon production and fluid withdrawal from storage systems, diverged significantly. Unlike carbon dioxide, desorption isotherms of the n-butane/n-hexane mixture did not follow the same trajectory as adsorption. Consequently, capillary evaporation pressures of the mixture could not be identified from the measured isotherms, indicating a distinct confinement-induced phase transition characteristic of multicomponent systems. Additionally, selective adsorption and desorption were found to be composition-driven rather than wettability-driven. These findings underscore the complexities of fluid storage and withdrawal in nanoporous media, offering valuable insights into optimizing storage applications in unconventional formations.

1 Introduction

The phase behavior of fluids under confinement differs significantly from bulk behavior due to enhanced fluid-solid and fluid-fluid interactions [1,2]. In nanoporous media, vapor-liquid phase transitions, such as capillary condensation and evaporation, occur isothermally at pressures lower than the bulk saturation pressure [3–5]. These transitions exhibit hysteresis under specific thermal and geometric conditions, characterized by distinct capillary condensation and evaporation pressures [6–8]. However, as temperature increases, hysteresis diminishes, and confined fluids transition to a reversible phase behavior before reaching the supercritical state [2,9].

Understanding the physical adsorption and phase behavior of fluids in nanoporous media is crucial for applications such as carbon capture [10–12], gas storage [13,14], and hydrocarbon recovery from unconventional reservoirs [15,16]. In carbon capture technologies, CO_2 adsorption and desorption are widely used to evaluate and design solid sorbents due to CO_2's strong affinity and rapid diffusion in small pores [10–12]. For gas storage systems, adsorption governs the amount of fluid stored, directly impacting storage efficiency [13]. In contrast, desorption regulates fluid withdrawal, influencing extraction feasibility and recovery efficiency [13]. These adsorption and desorption processes are therefore key to optimizing hydrogen and natural gas recovery performance, particularly in systems involving repeated injection and production cycles. Furthermore, incorporating confinement effects improves the accuracy of hydrocarbon volume estimation in shale and tight reservoirs compared to traditional methods that neglect these effects [16].

The confinement-induced phase transition of pure fluids, such as carbon dioxide (CO_2) [17,18] and hydrocarbons [4,9,19–22], has been extensively studied to improve the current understanding on how confinement alters fluid behavior. These studies have systematically explored the effects of pore size [21,23], pore shape [24], and wettability [25,26] on the confined phase behavior. For example, Salim et al. [17,18] investigated the impact

* Corresponding author: nan@uwyo.edu

of pore size on the confined phase behavior of subcritical and supercritical CO_2 in MCM-41 materials using a gravimetric method. Wang et al. [24] demonstrated the impact of pore shape and geometry on CO_2 storage capacity, while Nguyen et al. [25,26] studied the effect of wettability by comparing the phase behavior of pure alkanes in hydrophilic and hydrophobic nanoporous systems.

In contrast, despite the prevalence of fluid mixtures in geological formations, experimental studies on their confined phase behavior remain scarce [3,27–32]. Unlike pure fluids, multicomponent systems introduce additional complexity due to selective adsorption, competitive molecular interactions, and modified phase transition mechanisms [7,27]. For example, selective adsorption can alter bulk-vapor composition depending on the amount of nanoporous material present [27,33]. Wettability further complicates fluid mixture behavior by modulating fluid-solid affinity. However, its impact on multicomponent systems remains poorly understood. This knowledge gap hinders accurate predictions for subsurface storage in unconventional reservoirs, emphasizing the need for further investigation.

The present study attempts to fill this gap by examining the confined phase behavior of CO_2 and a binary hydrocarbon mixture (90 mol% n-butane and 10 mol% n-hexane) in MCM-41 nanoporous materials with a pore size of 8 nm under different wetting conditions. MCM-41, a silica-based nanoporous material, offers an ideal model for probing the confinement effects due to its well-defined pore structure and tunable surface chemistry. The original hydrophilic MCM-41 sample was modified with hexamethyldisilazane (HMDS), generating a hydrophobic counterpart to examine the impact of wettability on the storage capacity and thermodynamic properties. Adsorption (ADS) and desorption (DES) isotherms of pure CO_2 and the fluid mixture were measured in hydrophilic and hydrophobic samples at varying temperatures using a patented nano-condensation apparatus [34,35].

The results from this study provide valuable insights into the confined phase behavior of fluids in nanopores, emphasizing key differences between single- and multicomponent systems. While the adsorption behavior of the hydrocarbon mixture resembles that of pure CO_2, the desorption process diverges significantly, with implications for gas withdrawal from storage systems. In addition, the hydrophilic sample demonstrated enhanced storage capacity, underscoring the importance of surface chemistry in optimizing subsurface storage. Notably, selective adsorption and desorption were found to be primarily driven by fluid composition rather than wettability. These findings provide a critical understanding of confined fluid behavior for improving the efficiency of CO_2 capture employing nanoporous sorbents and hydrocarbon recovery in unconventional reservoirs.

The remainder of the paper is structured as follows. Section 2 details the materials and method employed in this study. Section 3 presents the ADS and DES isotherms of CO_2 and an n-butane/n-hexane binary mixture (90 mol% n-butane) measured in hydrophilic and hydrophobic MCM-41 samples. This section also examines the effects of wettability and fluid composition on the confined phase behavior. Finally, Section 4 summarizes key findings and offers recommendations for future research.

2 Materials and method

2.1 Materials

This study investigates the phase behavior of CO_2 as a pure fluid and a binary mixture of n-butane and n-hexane as a multicomponent system. High-purity gaseous CO_2 (>99%) was obtained from Airgas, Inc. The binary mixture, consisting of 90 mol% n-butane (Airgas, Inc., > 99% purity) and 10 mol% n-hexane (Sigma Aldrich, > 99% purity), was prepared using an in-house gravimetric gas-mixing apparatus. The final composition of the mixture was verified using a high-pressure/high-temperature gas chromatograph from Agilent Technologies, Inc.

The confined phase behavior of fluids was examined in hydrophilic and hydrophobic MCM-41 materials with an 8 nm pore size. The MCM-41 adsorbent (Glantreo, Ltd) is a well-characterized hydrophilic nanoporous material with uniform, non-interconnected cylindrical pores. The original MCM-41 sample was chemically treated with hexamethyldisilazane (HMDS) (Thermo Fisher Scientific) at 55 °C for 20 hours, following a detailed procedure described in the literature [36,37], to create a hydrophobic counterpart. This treatment replaced hydrophilic silanol [-Si(OH)] groups with hydrophobic trimethylsilyl (TMS) moieties [$-Si(CH_3)_3$] while preserving the original pore structure.

Comprehensive material characterization was conducted in prior studies [25,26]. Wettability was evaluated by measuring the contact angles of water droplets on compacted sample tablets, as shown in Fig. 1. The average pore size, surface area, and pore volume were determined using the Brunauer-Emmett-Teller (BET) and Barrett-Joyner-Halenda (BJH) [38] techniques via nitrogen adsorption and desorption isotherms at 77 K. Table 1 presents the measured pore properties.

Table 1. Characteristics of the hydrophilic and hydrophobic MCM-41 materials.

Property	Hydrophilic MCM-41	Hydrophobic MCM-41
BJH pore size (nm)	7.830	7.828
BET surface area (m^2/g)	164.1	131.3
BJH pore volume (cm^3/g)	0.993	0.771

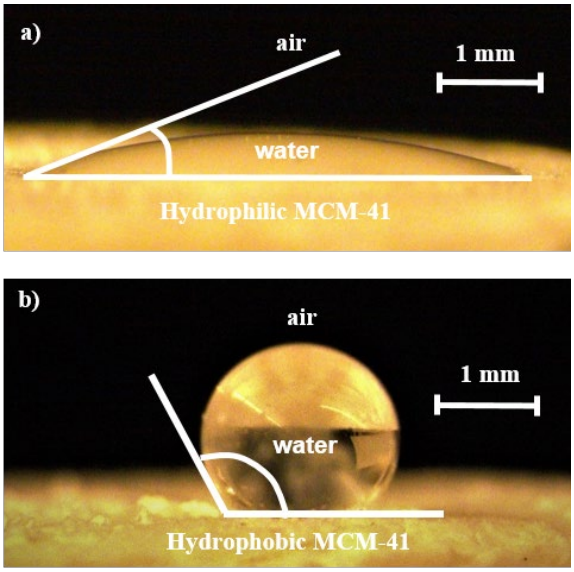

Fig. 1. Contact angles of a) water on the hydrophilic MCM-41 sample and b) water on the hydrophobic MCM-41 sample [26].

2.2 Experimental setup and procedure

A patented nano-condensation apparatus [23,34] was used to investigate the confined phase behavior of pure and multicomponent fluids in nanoporous media. This apparatus precisely measures ADS and DES isotherms by directly quantifying the amount of fluid adsorbed onto the pore walls while monitoring the corresponding bulk pressures. Previous work has validated its accuracy, with a systematic error of only ±1% [27]. A detailed description of the apparatus can be found in the literature [23,34].

The hydrophilic and hydrophobic MCM-41 samples were packed into two titanium core holders, which were suspended in an environmental chamber using balances positioned at the top. The chamber temperature was controlled by a thermocouple-regulated system. The core holders were connected via tubing to an external gas cylinder and vacuum pump, with automated valves and pressure transducers for precise control and monitoring.

For ADS measurements, small fluid doses were intermittently injected from the gas cylinder into the core holders. After each injection, the system equilibrated for approximately two hours, with mass and pressure recorded in real time via a custom LABVIEW program. DES experiments followed the reverse process, gradually withdrawing fluid using the vacuum pump.

The representative isotherms for pure fluids revealed distinct vapor-liquid phase transitions in confined spaces and their bulk counterparts (see Fig. 2). Under confinement, the capillary condensation and evaporation of fluids were characterized by abrupt changes in mass at intermediate pressures on the ADS and DES isotherms, respectively. The inflection points corresponding to these sudden transitions were defined as the capillary condensation pressure (P_a) during ADS and the capillary evaporation pressure (P_d) during DES [9,23]. The method for identifying inflection points using the Lorentzian function can be found in the literature [23,27]. Depending on pressure and temperature conditions, P_a and P_d might exhibit either hysteresis or reversible transitions, as shown in Fig. 2. By contrast, the bulk-phase transitions appeared as nearly vertical mass changes at the end of the ADS isotherms and the onset of the DES process, reflecting a sharp and reversible phase change without hysteresis.

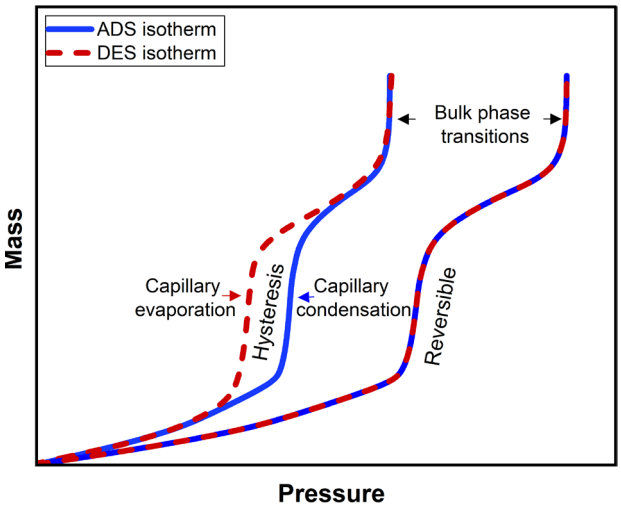

Fig. 2. Representative adsorption-desorption isotherms of pure fluids illustrating two types of phase behavior: a superimposed hysteresis transition (left) and a reversible transition (right). In the hysteresis case, capillary condensation and evaporation occur at different pressures, whereas in the reversible process, these pressures coincide.

3. Results and discussion

3.1 Carbon dioxide isotherms

This section analyzes the ADS and DES isotherms of CO_2 in hydrophilic and hydrophobic MCM-41 samples with an 8 nm pore size at 10 °C. Fig. 3 presents the experimentally measured isotherms, and Table 2 summarizes the capillary condensation (P_a) and evaporation (P_d) pressures. The effects of wettability on the confinement-induced phase behavior of CO_2 were examined to evaluate its storage potential in nanoporous media.

As shown in Fig. 3, the ADS and DES isotherms of CO_2 at 10 °C exhibit nearly identical trajectories, indicating reversible phase behavior under confinement with negligible hysteresis. As a result, P_a and P_d are comparable, at approximately 40 bar (see Table 2), in both hydrophilic and hydrophobic materials. In addition, P_a and P_d for CO_2 at 10 °C are lower than the bulk saturation pressure of 45 bar reported by the National Institute of Standards and Technology (NIST). This reduction in saturation pressure is attributed to the intense fluid-fluid and fluid-solid interactions under confinement. Such behavior is particularly significant for advanced gas storage technologies, where it could lower pressure requirements in high-pressure gas storage systems.

Capillary condensation and evaporation pressures of CO_2 in MCM-41 samples are represented as P_{a1} and P_{d1} for the hydrophilic sample and P_{a2} and P_{d2} for the

hydrophobic counterpart. The results in Table 2 show that P_{a2} and P_{d2} are slightly higher than P_{a1} and P_{d1}, consistent with findings reported by previous studies [25,26]. Although the variation between P_{a1} and P_{a2} was insignificant, it exceeded the system error of 1% [27]. The higher capillary condensation and evaporation pressures in the hydrophobic sample imply that its nanopores reached saturation with liquid-like CO_2 later than those in the hydrophilic sample. This phenomenon reflects the stronger fluid-solid intermolecular interactions between CO_2 and the hydrophilic surfaces.

Table 2. Capillary condensation (P_a) and evaporation (P_d) pressures of CO_2 in hydrophilic and hydrophobic MCM-41 samples with an 8 nm pore size.

Temperature (°C)	Bulk saturation pressure P_b (bar)	Hydrophilic MCM-41		Hydrophobic MCM-41	
		P_{a1} (bar)	P_{d1} (bar)	P_{a2} (bar)	P_{d2} (bar)
10	45.02	40.00	40.09	40.66	40.54

In addition to its effects on capillary condensation and evaporation pressures, wettability significantly governs the amount of adsorbed fluid in nanoporous materials. As shown in Fig. 4, the initial ADS sections demonstrate a more pronounced increase in the adsorbed mass for the hydrophilic sample compared to that for the hydrophobic one. In other words, more CO_2 was adsorbed onto the surfaces of the hydrophilic nanopores than onto their hydrophobic counterparts. This behavior is attributed to the stronger adsorption forces between the CO_2 molecules and the hydrophilic surfaces of the solid [39]. The weak interactions between CO_2 and the hydrophobic pores resulted in less CO_2 stored in the oil-wet nanoporous material. Fig. 4 compares the mass of CO_2 stored in the hydrophilic and hydrophobic MCM-41 samples at 10 °C before approaching the capillary condensation. The mass difference between the two samples ($m_1 - m_2$) is approximately 1 gram. These observations align with previous research indicating that wettability significantly impacts the physical adsorption of fluids in nanoporous materials [25,26].

Notably, the measured isotherms of CO_2 during the initial ADS and final DES processes exhibited distinct overlap in both hydrophilic and hydrophobic materials (see Fig. 3). This behavior suggests that CO_2, and potentially other pure gases, can be nearly fully recovered from the nanoporous storage system, regardless of the wettability of the material. The close alignment between the ADS and DES transitions indicates that the system reaches a near-complete recovery, leaving only minimal residual gas in the nanopores. This observation underlines the reversibility and efficiency of the adsorption-desorption process for pure fluid storage, emphasizing its potential for achieving high recovery rates in practical applications.

3.2 Multicomponent fluid isotherms

The phase behavior of multicomponent fluids under confinement was investigated through the phase transitions of an n-butane/n-hexane mixture containing 90 mol% n-butane. Fig. 5 presents the measured ADS isotherms of the binary mixture in the 8 nm hydrophilic and hydrophobic MCM-41 samples at three temperatures (10, 20, and 30 °C). The corresponding capillary condensation pressures (P_a) derived from these isotherms are tabulated in Table 3 and plotted in Fig. 6. The experimentally measured DES isotherms are shown in Fig. 7.

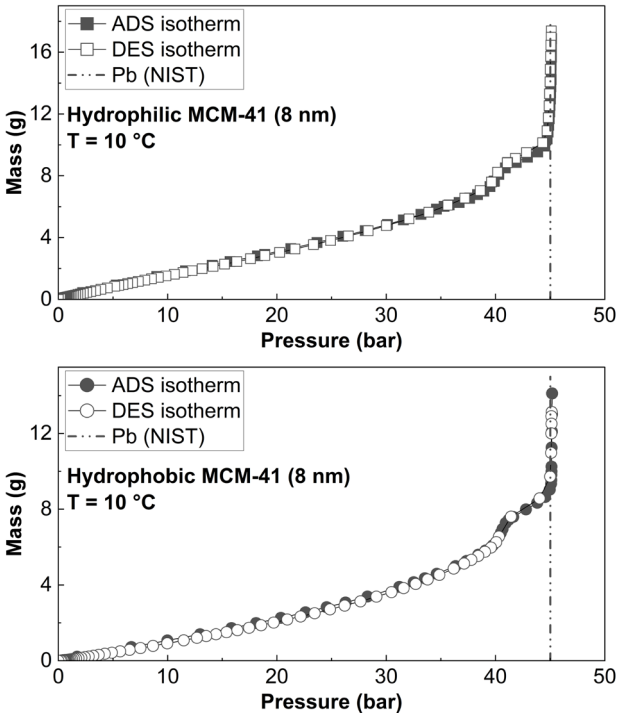

Fig. 3. Experimentally measured ADS and DES isotherms of CO_2 in hydrophilic and hydrophobic MCM-41 (with 8 nm pore size) samples at 10 °C. Solid symbols represent the ADS data, while hollow ones denote the DES data.

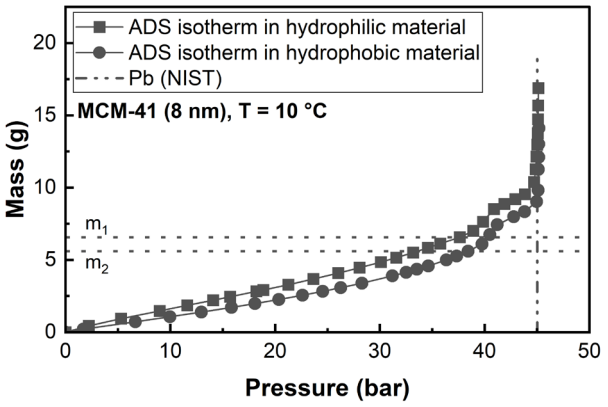

Fig. 4. The mass variations of adsorbed CO_2 in nanoporous materials with different wetting states.

During the ADS process, the confined phase behavior of the n-butane/n-hexane mixture (90 mol% n-butane) exhibited similarities to pure CO_2. As shown in Table 3

and Fig. 6, the vapor-liquid phase transition of the binary mixture in confined spaces occurred at lower pressures than in their bulk counterparts under isothermal conditions. For example, the bulk bubble point pressure (P_b) of the n-butane/n-hexane mixture containing 90 mol% n-butane at 10 °C, calculated using the PC-SAFT EOS [40,41], was 1.347 bar. Meanwhile, its capillary condensation pressures in the hydrophilic (P_{a1}) and hydrophobic (P_{a2}) MCM-41 samples with a pore size of 8 nm were 1.002 and 1.004 bar, respectively. Although P_{a1} was slightly lower than P_{a2}, this difference was negligible, as both values converged at 30 °C (see Table 3).

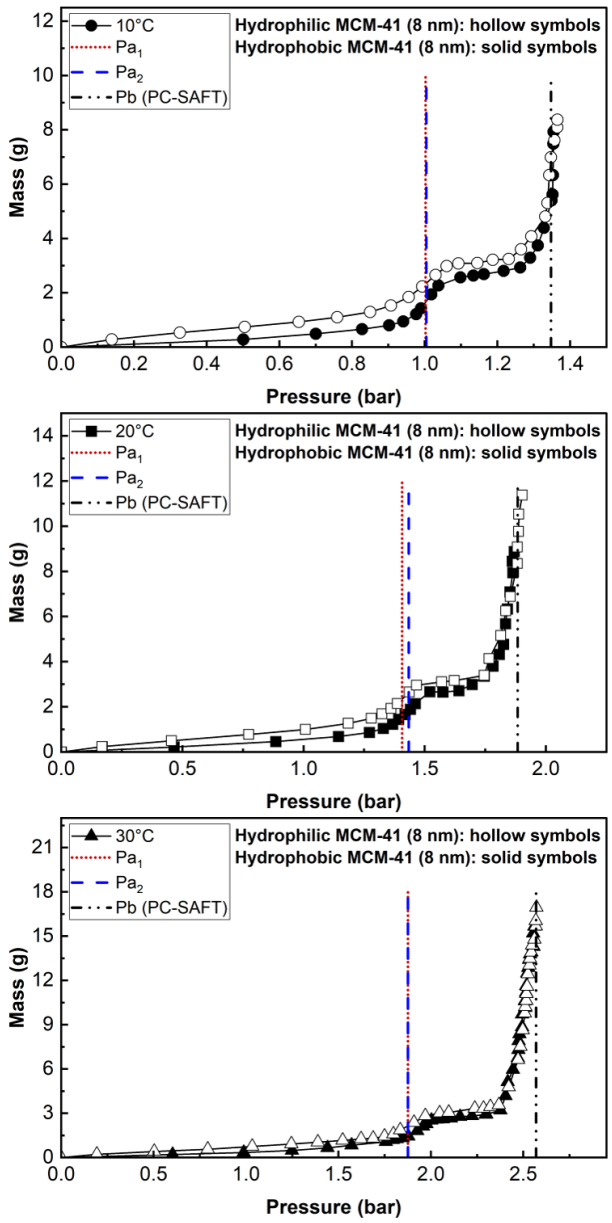

Fig. 5. Comparison of the effect of wettability on ADS isotherms of n-butane/n-hexane mixture (90 mol% n-butane) in hydrophilic and hydrophobic MCM-41 (8 nm) samples.

The effect of wettability on the confinement-induced phase behavior of multicomponent fluids was most apparent during the initial ADS stage. As shown in Fig. 5, the increase in the adsorbed mass was more noticeable in the hydrophilic sample than in the hydrophobic one, implying stronger fluid-solid interactions of the silanol [-Si(OH)] functional groups. This behavior of the n-butane/n-hexane mixture was consistent with that of pure CO_2.

Interestingly, no evidence of wettability-induced selective adsorption was observed. The bulk condensation behavior of the fluid mixture in hydrophilic and hydrophobic materials remained nearly identical (see Fig. 5). This phenomenon indicates that the adsorption ratios of n-butane and n-hexane were similar regardless of surface chemistry. In other words, variations in adsorption forces due to different surface functional groups were uniformly applied to all components, preventing preferential adsorption based on wettability.

At the later stage of the adsorption process, the bulk condensation of the fluid mixture did not follow a complete vertical trend (see Fig. 5). If additional fluid were introduced into the system, the bulk condensation pressure could exceed the pre-determined P_b (PC-SAFT). This hypothesis suggests that MCM-41 samples could elevate the bulk condensation pressure beyond the bubble point of the fluid mixture in the absence of nanoporous materials. As a result, n-hexane appears to be preferentially adsorbed, leaving more n-butane in the bulk phase. In this case, selective adsorption occurred due to the stronger adsorption forces of n-hexane rather than wettability effects. However, more experimental data are needed to confirm this behavior.

Unlike pure CO_2, the DES isotherms of the n-butane/n-hexane mixture deviated significantly from the ADS isotherms, exhibiting entirely unexpected behavior (see Fig. 7). Instead of a sharp capillary evaporation transition, the DES of the fluid mixture resembled a continuous emptying process, where the adsorbed mass decreased gradually and only dropped significantly near the end after the samples had been subjected to a prolonged vacuum. Consequently, capillary evaporation of the fluid mixture was not observed in the measured DES isotherms.

During the DES process of the n-butane/n-hexane mixture, a distinct hysteresis between ADS and DES isotherms was observed, highlighting a key difference between fluid mixtures and pure fluids. As previously noted, the final DES stage of pure CO_2 overlapped with the initial ADS process. However, these ADS and DES segments for the n-butane/n-hexane binary mixture were irreversible (see Fig. 7). This behavior can be attributed to selective desorption effects. Specifically, n-butane, with weaker interactions, desorbed more readily, while n-hexane, the heavier component with stronger adsorption affinity, remained trapped in the pores. As a result, selective desorption led to pore-blocking effects, making it more challenging to withdraw gas mixtures stored in nanoporous media or unconventional reservoirs. This phenomenon could leave a substantial fraction of retained fluid even after subjecting the samples to a strong vacuum for an extended period of time.

Table 3. Measured capillary condensation pressures (P_a) of n-butane/n-hexane mixture (90 mol% n-butane) in (1) hydrophilic and (2) hydrophobic MCM-41 samples.

Temperature (°C)	P_b (bar)	P_{a1} (bar)	P_{a1} standard error (bar)	P_{a2} (bar)	P_{a2} standard error (bar)	Variation P_{a2}-P_{a1} (bar)
10	1.347	1.002	±0.005	1.004	±0.001	0.002
20	1.883	1.406	±0.006	1.434	±0.007	0.028
30	2.569	1.876	±0.009	1.876	±0.004	0.000

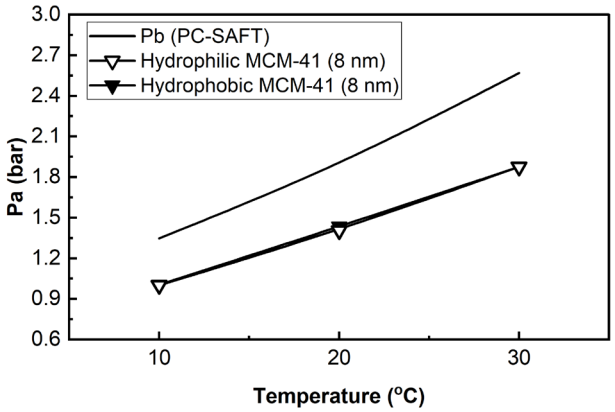

Fig. 6. Comparison of the effect of wettability on capillary condensation pressure of n-butane/n-hexane mixture (90 mol% n-butane) in MCM-41 materials at varying temperatures.

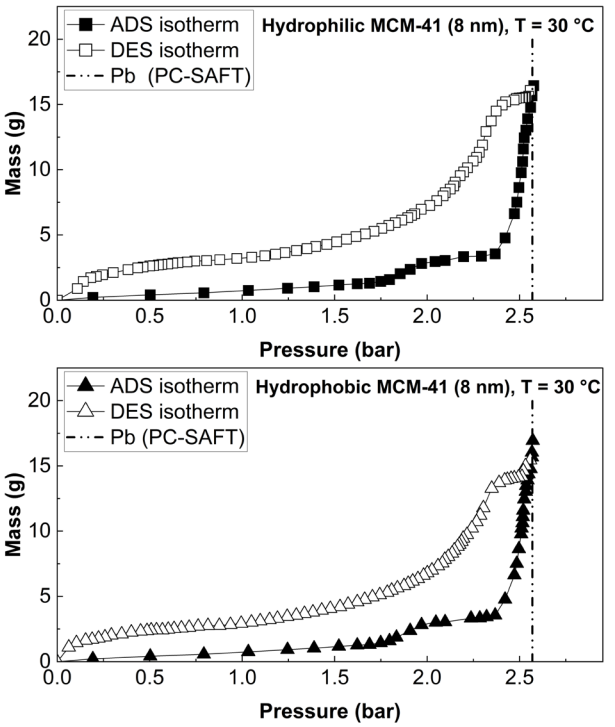

Fig. 7. ADS and DES isotherms of n-butane/n-hexane mixture (90 mol% n-butane) in MCM-41 hydrophilic and hydrophobic materials with an 8 nm pore size at 30 °C.

4 Conclusions

This study examines the confined phase behavior of pure and multicomponent fluids in nanoporous media, focusing on the effects of wettability and fluid composition on adsorption and desorption. We analyzed the vapor-liquid phase transitions of pure CO_2 and an n-butane/n-hexane binary mixture (90 mol% n-butane) in hydrophilic and hydrophobic MCM-41 materials with a pore size of 8 nm. The results show that hydrophilic materials adsorbed and stored more CO_2 and hydrocarbons than hydrophobic ones. While adsorption trends are largely similar between pure CO_2 and the mixture, desorption behavior differs significantly. The inability to identify capillary evaporation pressures for the mixture suggests a confinement-induced phase transition unique to multicomponent systems. Moreover, the observed selective adsorption and desorption were driven by fluid composition rather than wettability. Additional experimental data are required to validate this observation. These findings provide critical insights for optimizing carbon capture, gas storage, and hydrocarbon recovery in unconventional reservoirs.

The authors gratefully acknowledge the financial support of Hess Corporation and the University of Wyoming.

References

1. T. Horikawa, D. D. Do, and D. Nicholson, Adv. Colloid Interface Sci. **169**, 40 (2011).
2. E. Barsotti, S. P. Tan, S. Saraji, M. Piri, and J. H. Chen, Fuel **184**, 344 (2016).
3. E. Barsotti, S. Saraji, S. P. Tan, and M. Piri, Langmuir **34**, 1967 (2018).
4. R. M. Alloush, K. V. Sharma, and M. Piri, Phys. Chem. Chem. Phys. **19**, (2023).
5. K. V. Sharma, R. M. Alloush, O. Salim, and M. Piri, Phys. Chem. Chem. Phys. 18162 (2024).
6. E. Barsotti, S. P. Tan, M. Piri, and J. H. Chen, Fuel **263**, 116441 (2020).
7. X. Qiu, H. Yang, M. Dejam, S. P. Tan, and H. Adidharma, J. Phys. Chem. C **125**, 5802 (2021).

8. P. I. Ravikovitch and A. V. Neimark, Colloids Surfaces A Physicochem. Eng. Asp. **188**, 11 (2001).
9. E. Barsotti, S. P. Tan, M. Piri, and J. H. Chen, Langmuir **34**, 4473 (2018).
10. S. Rezaei, A. Liu, and P. Hovington, Catal. Today **423**, 114286 (2023).
11. F. Raganati, F. Miccio, and P. Ammendola, Energy and Fuels **35**, 12845 (2021).
12. C. Chao, Y. Deng, R. Dewil, J. Baeyens, and X. Fan, Renew. Sustain. Energy Rev. **138**, 110490 (2021).
13. R. E. Morris and P. S. Wheatley, Angew. Chemie - Int. Ed. **47**, 4966 (2008).
14. S. Alhasan, R. Carriveau, and D. S. K. Ting, Int. J. Environ. Stud. **73**, 343 (2016).
15. N. S. Alharthy, T. N. Nguyen, T. W. Teklu, H. Kazemi, and R. M. Graves, Proc. - SPE Annu. Tech. Conf. Exhib. **4**, 2705 (2013).
16. J. H. Chen, A. Mehmani, B. Li, D. Georgi, and G. Jin, SPE Middle East Oil Gas Show Conf. MEOS, Proc. **3**, 2208 (2013).
17. O. Salim, K. V. Sharma, and M. Piri, (2024).
18. O. Salim, K. V. Sharma, and M. Piri, J. CO2 Util. **92**, 103017 (2025).
19. J. H. Yun, T. Düren, F. J. Keil, and N. A. Seaton, Langmuir **18**, 2693 (2002).
20. H. Yang, K. Jayaatmaja, M. Dejam, S. P. Tan, and H. Adidharma, Langmuir **38**, 2046 (2022).
21. K. V. Sharma, R. M. Alloush, and M. Piri, Microporous Mesoporous Mater. **351**, 112459 (2023).
22. J. Ally, S. Molla, and F. Mostowfi, Langmuir **32**, 4494 (2016).
23. R. Alloush, K. Sharma, and M. Piri, J. Mol. Liq. 119894 (2022).
24. S. Wang, O. Salim, and M. Piri, Mater. Today Sustain. **29**, 101076 (2025).
25. A. T. T. Nguyen, K. V Sharma, and M. Piri, (2024).
26. A. T. T. Nguyen, K. V Sharma, and M. Piri, in *Soc. Core Anal.* (2024).
27. A. T. T. Nguyen, K. V. Sharma, and M. Piri, Ind. Eng. Chem. Res. **63**, 15948 (2024).
28. S. Luo, J. L. Lutkenhaus, and H. Nasrabadi, Fluid Phase Equilib. **487**, 8 (2019).
29. S. Luo, J. L. Lutkenhaus, and H. Nasrabadi, J. Pet. Sci. Eng. **163**, 731 (2018).
30. M. A. Khoshooei, D. Sharp, Y. Maham, A. Afacan, and G. P. Dechaine, Thermochim. Acta **659**, 232 (2018).
31. H. Cho, M. H. Bartl, and M. Deo, Energy and Fuels **31**, 3436 (2017).
32. X. Qiu, S. P. Tan, M. Dejam, and H. Adidharma, Chem. Eng. J. **405**, 127021 (2021).
33. X. Qiu, S. P. Tan, M. Dejam, and H. Adidharma, Phys. Chem. Chem. Phys. **21**, 224 (2019).
34. M. Piri, E. Barsotti, and S. Saraji, 15/588094 (2019).
35. R. Alloush, M. Piri, and E. W. Lowry, US 2022/0357256 A1 (2022).
36. S. Luo, J. L. Lutkenhaus, and H. Nasrabadi, Langmuir **32**, 11506 (2016).
37. S. Luo, H. Nasrabadi, and J. L. Lutkenhaus, AIChE J. **62**, 1772 (2016).
38. E. P. Barrett, L. G. Joyner, and P. P. Halenda, Vol. Area Distrib. Porous Subst. **73**, 373 (1951).
39. J. N. Israelachvili, *Intermolecular and Surface Forces: Third Edition* (2011).
40. J. Gross and G. Sadowski, Ind. Eng. Chem. Res. **40**, 1244 (2001).
41. W. B. Kay, R. L. Hoffman, and O. Davies, J. Chem. Eng. Data **20**, 333 (1975).